Optics Letters

High-level integration of three-dimensional microcoils array in fused silica

CHAO SHAN, FENG CHEN,* QING YANG, YANYANG LI, HAO BIAN, JIALE YONG, AND XUN HOU

[1]State Key Laboratory for Manufacturing System Engineering & Key Laboratory of Photonics Technology for Information of Shaanxi Province, School of Electronics & Information Engineering, Xi'an Jiaotong University, No 28 Xianning West Road, Xi'an 710049, China
*Corresponding author: chenfeng@mail.xjtu.edu.cn

Received 7 May 2015; revised 28 June 2015; accepted 4 August 2015; posted 5 August 2015 (Doc. ID 240521); published 26 August 2015

Rapid and facile creation of three-dimensional (3D) microcoils array in a "lab-on-a-chip" platform is a big challenge in micromachining. Here we report a method based on an improved femtosecond-laser wet-etch (FLWE) technology and metal-microsolidifying process for the fabrication of 3D microcoils array inside fused silica. Based on this approach, we fabricated microcoil arrays such as 3 × 3 O-shaped microcoils array and 4 × 4 liner microcoils array. By injecting high-melting-point alloy, the electrocircuit of microcoils array can hardly be disconnected. The microcoils array also exhibits good uniformity and a high integration level. It shows promise as a real application device.

OCIS codes: (220.4000) Microstructure fabrication; (220.4241) Nanostructure fabrication; (350.3390) Laser materials processing; (230.4000) Microstructure fabrication.

http://dx.doi.org/10.1364/OL.40.004050

Microcoil array has a wide variety of applications. Typical examples include parallel magnetic-resonance (MR) imaging and spectroscopy, chip–nuclear magnetic-resonance (NMR) biosensor for detection and molecular analysis of cells, and micromanipulation [1–4]. Especially in MR microscopy, as a detector, microcoil arrays can achieve high-resolution MR images of human skin successfully [5]. Compared with a single microcoil, which likes bones of a body for the micro-electromechanical systems (MEMS), single microcoil has many shortages as a real application device. Although a single microcoil can be fabricated as a microsensor or a micro-actor [6,7], the scope of influence is small, and the intensity and the force of magnetic field is weak. Therefore, considering the practical factors of integrated chips, the research of microcoil-array fabrication is becoming the key and hot spot in the microsystem development.

Recently, many efforts have been made focusing on the fabrication of microcoil arrays [2,8–10]. The fabrication of microcoil arrays is developed on the basis of the single microcoil structure. At present, the processes to fabricate microcoil arrays include multilayer photolithography and electroplating, winding a metal wire around a yoke, and creating helical-conducting paths on a cylinder [11–15]. However, these processing methods are not only lacking of flexibility, low integration degree, but also very difficult integration with other systems, especially in micro-total analysis systems (μTAS). Because microcoil arrays inside of materials cannot be fabricated by these methods. In previous studies [16,17], we proposed a fabrication of complex three-dimensional (3D) microcoils in fused silica by femtosecond-laser wet-etch (FLWE) technology and metal microsolidifying process. This one-microcoil fabrication method provides a new thought and solution to processing microcoil arrays in fused silica.

However, compared with the single-microcoil fabrication, the processing difficulty mainly exists in the device uniformity, consistency, and how to improve the integration level of microcoil arrays. Another factor limiting microcoil-array applications is the low melting point of the metal microsolidifying process. The low melting point metal cannot afford high current, which makes the microcoil circuit break easily. In this Letter, the above-mentioned problems have been solved.

In this Letter, we fabricate high-integration level on-chip 3D microcoil arrays with good uniformity and consistency inside fused silica based on femtosecond-laser wet-etch (FLWE) technology and a metal microsolidifying process. This Letter pays more attention to the practical application of the 3D microcoil-array device properties and functionality. A kind of alloy with higher melting point than metal gallium, which we used in our previous studies, has been used in the metal microsolidifying process. This alloy mainly contains metal stannum, bismuth, and lead. The mainly reason why we choose this alloy is that it has appropriate melting point (92.6°C). This melting point means being able to take more current, and does not make the microsolidifying process become very difficult. This new alloy also has lower viscosity conductive, and can be easily imported into the microchannels. Thus, the utility and application scope of the microcoil array fabricated by FLWE will be greatly improved.

The microcoil-manufacturing process proposed in [17] includes two steps: production of 3D microchannels, and injection with alloy into the channels in the fused silica. What is different is here we use two-step wet etch. The coil sample was immersed in a solution of 5% HF for 1 h (in room-temperature deionized water dilution). Here we call this process pre-etching. This contacts the entire femtosecond-laser-irradiated pattern

0146-9592/15/174050-04$15/0$15.00

with HF sufficiently but not intensely. Then, we put this sample into another solution of 10% HF. Under this approach, it is possible to improve the uniformity and smoothness of the microchannels' inner wall to reduce the flow resistance of liquid metal. Another difference is the temperature maintained at about 120°C by high-temperature drying box during injection.

Compared with single microcoil, the difficulty of fabricate microcoil arrays is how to get very long microchannel with great uniformity. By creating a series of laser-irradiated lines that connect a sample surface and the internal structures, extra access ports are prepared by chemical process [16]. In this case, HF acid solutions can directly penetrate into the central parts of the channels rapidly. Then, each part of the microchannels can be etched simultaneously. Under this approach, the fabrication of the entire array can be considered as each part fabricated respectively. By the same conditions of laser irradiation and chemical etching, microchannels with long lengths and great uniformity have been realized.

Figure 1(c) is a linear inductance 4×4 microcoils array filled with alloy metal. For a single microcoil, the length of helical portion of the channel is about 400 μm. The number of turns is 5. The diameter of the alloy wire is 35 ± 1 μm. The radius and pitch of the coils are both 80 μm.

An O-shaped inductance 3×3 microcoil array filled with alloy metal is shown in Fig. 1(d). For a single microcoil, the radius of the O-shaped circle is 200 μm, and the radius of each of the coils is 75 μm. The number of turns is 9. The diameter of the alloy wire is 36 ± 1 μm.

The inductance, L, of the helical microcoils can be estimated by Wheeler's formula:

$$L = \frac{10\pi\mu_0 N^2 r^2}{9r + 10h_{\mathrm{coil}}}. \tag{1}$$

Here, $\mu_0 = 4\pi \times 10^{-7}\ \mathrm{Hm}^{-1}$ is the permeability in free space, N is the number of turns, r is the coil radius, and h_{coil} is the length of the coil. The U-shaped inductance microcoils array of the alloy metal coil is calculated to be 24.9 nH. The direct-current resistance of the microcoils is 1.75 Ω. The inductance of the O-shaped coil array is calculated to be 12.8 nH. The direct-current resistance of the microcoils is 2.06 Ω.

Uniformity and consistency is the key performance of the array device. A single set of repeated well will determine the whole array device quality, but also the evaluation of device performance standard. We are preparing microcoil arrays prepared in two types, with uniformity and good consistency. First, of all reflected uniformity in a single device, we can see that for these helical micro-coils, the diameter size error is only 1 micron. Second, the structure and size of each unit in the array of devices, including diameter, pipe diameter size, spacing, and the error, is less than 2 microns.

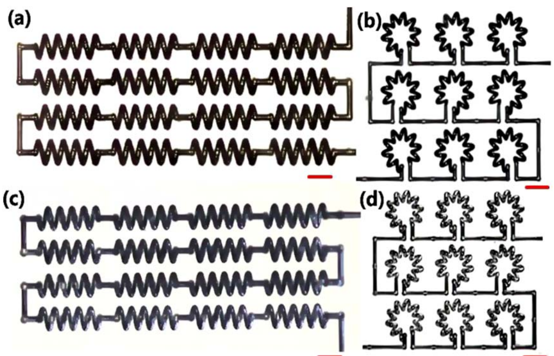

Fig. 1. (a) Liner microchannel array etched by HF. (b) O-shaped microchannels array etched by HF. (c) Liner microcoils array injected with alloy metal. (d) O-shaped microcoil array injected with alloy metal. The scale bar equals 200 μm.

The key indicator of another decision array-device performance is the integration level of the device. We know that the micromagnetic field coil device has a relatively small range. If each unit microcoil distance is too far away, the magnetic field cannot be effectively overlapped. In the whole array range, it also can generate uneven magnetic-field distribution, or even blank positions. Therefore, regulating each unit in the array microcoil in a range is very necessary and critical. Traditional microcoil-array winding-machine preparation method, limited by the winding-machine tip size, cannot control the distance of adjacent microcoil at the micron scale. But this problem can be solved well by the FLWE process. The integration level of device is greatly improved.

The integration level is embodied in two aspects: one is reflected in the distance of each unit of microcoils array, and another is reflected in the spatial layers. Figure 2 shows the distance of two kinds of microcoil arrays. In Fig. 2(a), the longitudinal spacing of the line microcoil array is 41.96 μm. In Fig. 2(b), the longitudinal spacing of the O-shape microcoils array is 33.54 μm, and the horizontal spacing is 153.5 μm. Through the magnetic-field-simulation calculation, the effective magnetic-field range of one single microcoil can be generally known in several hundreds of microns. So the microcoil array we are processing can meet the requirements of magnetic-field superposition. At the same time, the distance of microcoils array can be controlled by a computer program to make the changes within a certain range. The distance between each microcoil can reach 10 μm of minimum.

Figure 3 is another kind manifesting the integration level, namely two parallel layers of microcoils in the space. In order to observe, the two microcoils are malposed. Figure 3(c) shows the image when the microscope is focusing on the microcoil's upper, and Fig. 3(d) shows the image when the microscope is focusing on the microcoil's lower. In our previous studies, although the microcoils are three-dimensional, the use of sample is still limited in a layer that is not true 3D. The design in this work can effectively use the sample thickness to make the use of samples three-dimensional become real. It also can improve the sample integration level multiplied. What's more, in the middle area of two parallel microcoil layers, microchannels, microcabins, or even more complex microfluidic units can be integrated. This approach makes the "lab-on-a-chip" platform

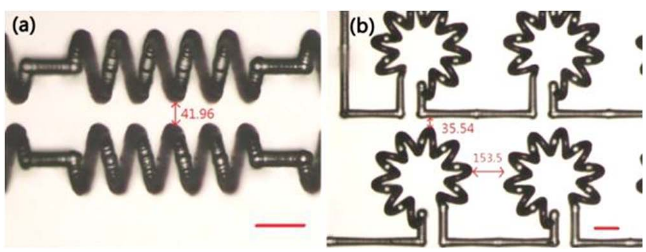

Fig. 2. Distance of each microcoil array. The scale bar equals 200 μm.

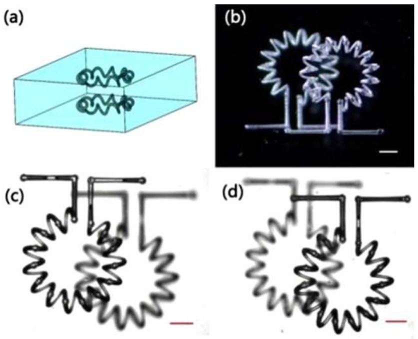

Fig. 3. (a) Schematic diagram of two parallel layers of O-shaped microcoils in the space. (b) Two parallel layers of O-shaped microchannels observed by digital camera. (c) Microscope focusing on the microcoil's upper. (d) Microscope focusing on the microcoil's lower. The scale bar equals 200 μm.

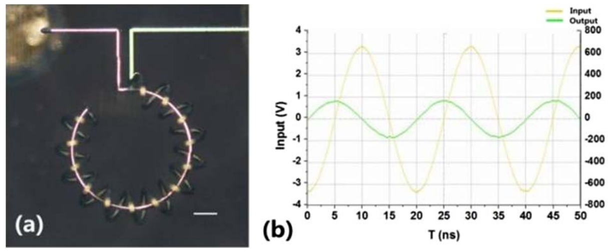

Fig. 5. (a) Rogowski microcoils. (b) The result of the relationships between the input signal and the output signal. The scale bar equals 200 μm.

density of integration improved greatly. It also makes more functional units integrated in smaller chips become possible.

The influence factors of microcoil-array applications also include the current transport capability of microcoil arrays. As we know, the magnetic field generated by microcoils is very weak. If the carrying current is small, it will be very difficult to generate the magnetic field strength of actual requirements. The gallium metal, used in our previous study, has a melting point that is about 29.7°C. The benefit of low melting point is easy metal microsolidifying, which can inject the molten metal to the microchannels easier. However, it also brought new problems, that at slightly higher than room temperature or under the action of the current thermal effect, the device will circuit break. It affects the device's normal use, which causes great impact and inconvenience of the microcoil application.

So we need a more appropriate melting point metal, which is a need of meeting requirements of the microcoil's high carrying current. And it will not make the metal microsolidifying process become too difficult. In this Letter, we finally chose a kind of alloy whose melting point is 92.6°C. A vacuum drying oven is used in the metal microsolidifying process to provide constant temperature 120°C for the entire system. This approach ensures the alloy melting and injected to the microchannels smoothly.

For the fabricated O-shaped microcoil array, we also test its ability of carrying current. Figure 4 shows the stable temperature of the sample surface after the current loaded. We can see when the current values reach close to 0.9 A, the temperature of sample surface is around the alloy melting temperatures. If the carrying current does not last very long, the microcoils array will not circuit break when the carrying current is over 1 A. Therefore, the scope of microcoil arrays carrying current has been greatly expanded. What's more, this high-melting-point alloy also can be used as a microheater. This microcoil array can be applied as a microheaters array.

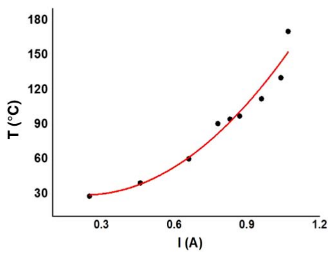

Fig. 4. Stable temperature of the sample surface after the current loaded.

At last, we fabricate a current microsensor named Rogowski microcoil to test the practicability of high-melting-point metal and the ability of electromagnetic induction. Figure 5(a) shows the Rogowski microcoils fabricated by FLWE and metal microsolidifying process.

After the fabrication of Rogowski microcoils, we connect the electrodes to the oscilloscope through a designed circuit, and a wire that connects high-frequency signal generator is through in the circle center of the Rogowski coil. In this way, the signal generator outputs a sine wave signal whose amplitude is 6.5 V and frequency is 50 MHz. The induced current of the Rogowski coil is also a sine wave signal of 400-mV amplitude and 50-MHz frequency. Figure 5(b) shows the result. The results not only proved the feasibility of the application of high melting point metal in microcoil, they also prove the feasibility of microcoil in practical application.

In summary, by means of FLWE technology and metal microsolidifying technology, 3D microcoil arrays can be achieved inside fused silica. The microcoil arrays with high integration level and uniformity for high-performance applications are realized, demonstrating the flexibility and universality of FLWE technology. Meanwhile, a broad spectrum of micro-electric systems will be promising, fabricated based on these compact and complex 3D microcoil arrays.

Funding. National Natural Science Foundation of China (NSFC) (51335008, 61275008, 61475124); Special-Funded Program on National Key Scientific Instruments and Equipment Development of China (2012YQ12004706).

REFERENCES

1. H. Lee, E. Sun, and D. Ham, Nat. Med. **14**, 869 (2008).
2. V. Badilita, K. Kratt, and N. Baxan, *IEEE 24th International Conference on Micro Electro Mechanical Systems (MEMS)* (IEEE, 2011), p. 809.
3. H. Lee, Y. Liu, and D. Ham, Lab Chip **7**, 331 (2007).
4. Y. F. Lee, K. Y. Lien, and H. Y. Lei, Biosens. Bioelectron. **25**, 745 (2009).
5. A. G. Webb, J. Magn. Reson. **229**, 55 (2013).
6. Y. Lu and H.-F. Ji, Sens. Actuators B **123**, 937 (2007).
7. C. Massin, G. Boero, and F. Vincent, Sens. Actuators A **97**, 280 (2002).
8. C. Ravat, M. Woytasik, and P. Y. Joubert, in *Solid-State Sensors, Actuators and Microsystems Conference*, Lyon, France, 2007, p. 583.

9. K. Kratt, V. Badilita, and T. Burger, J. Micromech. Microeng. **20**, 015021 (2010).
10. V. Shutov, E. Sandoz, and L. Howard, Sens. Actuators A **121**, 566 (2005).
11. S. Waselikowski, K. Kratt, and V. Badilita, Appl. Phys. Lett. **97**, 261105 (2010).
12. T. Dohi, K. Kuwana, and K. Matsumoto, in *Solid-State Sensors, Actuators and Microsystems Conference*, Lyon, France, 2007, pp. 1313–1316
13. M. J. K. Klein, T. Ono, and M. Esashi, J. Micromech. Microeng. **18**, 075002 (2008).
14. B. Lochel, A. Maciossek, and M. Rothe, Sens. Actuators A **54**, 663 (1996).
15. D. A. Seeber, R. L. Cooper, and L. Ciobanu, Rev. Sci. Instrum. **72**, 2171 (2001).
16. S. G. He, F. Chen, and Q. Yang, J. Micromech. Microeng. **22**, 105017 (2012).
17. F. Chen, C. Shan, and K. Liu, Opt. Lett. **38**, 2911 (2013).